Analysis and modeling of on-chip transformers under two ground conditions*

Wei Jiaju(韦家驹), Wang Zhigong(王志功)†, Li Zhiqun(李智群), and Tang Lu(唐路)

Institute of RF- & OE-ICs, Southeast University, Nanjing 210096, China

Abstract: Two fabricated on-chip transformers under different ground conditions (i.e., CG and IG types) have been measured to compare their different characteristics. With the aid of the electromagnetic (EM) solver, we have analyzed the differences from the electric and magnetic aspects, and different effects in these aspects can be described with the lumped capacitor and inductor from the perspective of the equivalent circuit model. A physics-based equivalent circuit model is proposed to model transformers under different ground conditions. In addition, the simple parameter extraction procedure for the corresponding model is also provided. All the model parameters are extracted and agree with the analysis. In order to verify the model's validity and accuracy, we have compared the modeled and measured S-parameters, and an excellent agreement has been found over a broad frequency range.

Key words: transformer; model; equivalent circuit; ground; on-chip; RFIC

DOI: 10.1088/1674-4926/33/6/065010 **EEACC:** 2570

1. Introduction

On-chip spiral transformers play an important role in RFIC designs and their characteristics should depend on the configurations in the measurements. A spiral transformer with 4 terminals can be measured in the 4-port[1] or 2-port[2] configurations. Actually, it is not convenient to measure a 4-port device by using a 2-port VNA (vector network analyzer), so applications of the transformer often adopt the 2-port configuration (2 terminals are connected to ground or virtual ground).

In the 2-port measurement, two ground-signal-ground (GSG) probes are applied to the ports of the device. For each port, one terminal connecting to "G" pad serves as the reference/ground of the other terminal connecting to "S" pad. Since two grounds of the two ports are connected together through the probe, cable, VNA, and then earth, it seems that whether to connect the two grounds together on the chip or not makes no difference. However, as demonstrated by EM simulations and measurements, the transformer response differs considerably in these two ground conditions which can be denoted as "common ground type (CG)" and "isolated ground type (IG)" for simplicity.

Although many works have been published on the modeling or characterization of on-chip transformers[1−9], most of them are based on the specific measurement type (i.e., CG or IG). To the best of the author's knowledge, the comparisons of the transformers under these two conditions are scarce. In this paper, the different characteristics of the transformers under different ground conditions are compared, analyzed and modeled over a broad frequency range.

2. Measurement and comparison

As shown in Fig. 1, two on-chip interleaved transformers under different ground conditions have been fabricated in a 0.18-μm 1P6M CMOS process with substrate resistivity of about 10 Ω·cm and top metal thickness of 2.34 μm. The line width and line spacing are 8 μm and 2 μm, respectively, and the outer diameter of the transformer is 236 μm. Based on the layout of the IG type, two strips with edge-to-edge separation

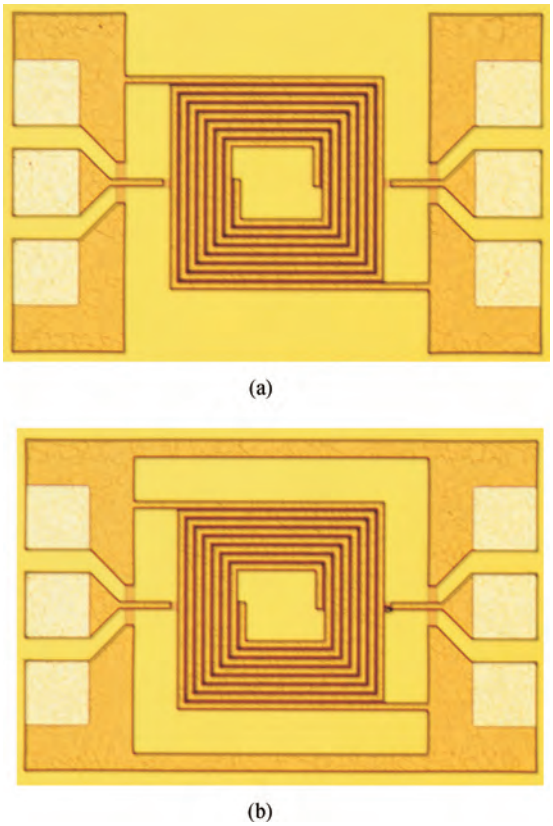

Fig. 1. Top view of the fabricated transformers. (a) IG type. (b) CG type.

* Project supported by the National Natural Science Foundation of China (No. 61106024).

† Corresponding author. Email: zgwang@seu.edu.cn

Received 25 December 2011

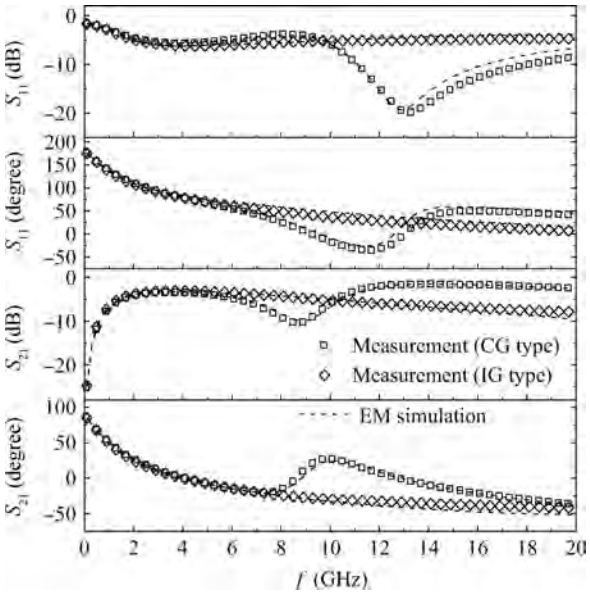

Fig. 2. S-parameter comparison between two types.

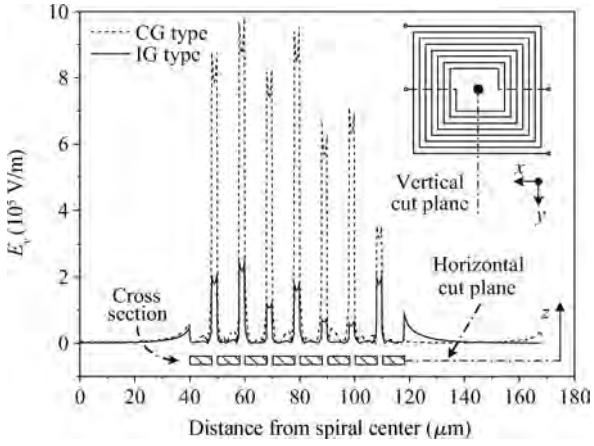

Fig. 3. Electric field intensity comparison between two types.

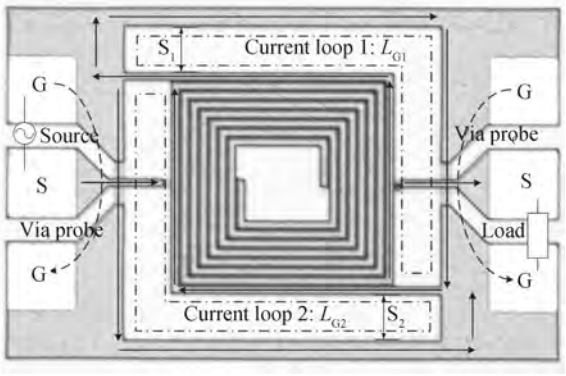

Fig. 4. Simple illustration of current distribution.

of 50 μm from the spiral and width of 20 μm are added in the CG type. 2-port S-parameters were measured and the pad parasitics were de-embedded from the measurement using the open pad structure.

The measured S-parameters (S_{11} and S_{21}) of the transformers are compared in Fig. 2. Because of symmetry and reciprocity, S_{22} and S_{12} are nearly identical to S_{11} and S_{21}, respectively, so we omit them for clarity. As demonstrated in Fig. 2, the response of the CG type shows sharp peaks and valleys while the IG type only shows a smooth response. Reference [3] did a qualitative analysis on this phenomenon from the viewpoint of the power transfer mechanism, while this paper will explain it from the circuit viewpoint quantitatively.

3. Analysis

In our analysis, a full-wave numerical electromagnetic (EM) field solver has been used. Based on the process parameters, we calibrate the solver's configuration and get an accurate EM simulation results compared with measurements in Fig. 2. With the tool, we will discuss the differences of the CG and IG types from the electric and magnetic aspects, and different effects in these aspects can be described with the lumped capacitor and inductor in the equivalent circuit model, respectively.

3.1. Electric field coupling

In order to gain more insights into the electric coupling between the primary and secondary coils, we compare the electric field intensity under different ground conditions by EM simulations. The simulation is applied along the line determined by the vertical and horizontal cut planes in Fig. 3. As shown in this figure, the normal component of electric field intensity forms a sharp peak between adjacent metal lines, while it falls back to about zero within or far away from the metal lines. From the circuit perspective, the energy stored in the electric field can be viewed as the one stored in an equivalent capacitance. Because the adjacent lines belong to different coils, this capacitance should belong to the mutual coupling capacitance between the primary and secondary coils.

In Fig. 3, it can be seen that the magnitude of electric field intensity in the CG type is several times (denoted as N, $N \approx$ 4–5) of that one in the IG type. Equivalently, the mutual coupling capacitance of the former is N^2($\approx$16–25) times of the latter and this can be approximately demonstrated by the extracted model parameters in Section 5. This is due to the fact that the energy is proportional to the square of electric field intensity, while proportional to the capacitance in the circuit model.

3.2. Magnetic field coupling

The current distribution of the transformer in the CG type is simply illustrated in Fig. 4. As shown in this figure, the currents form two loops around the transformer spiral, and the magnetic effects associated with both loops can be represented by two inductors (i.e., L_{G1} and L_{G2}). Each loop links one spiral coil to its corresponding strip, while the strips are connected via the testing pads. Thus, an equivalent inductor ($L_{G1} + L_{G2}$) should be introduced to link the transformer's primary and secondary coils at their grounding points in the circuit model.

With the aid of EM simulations, we change the areas of the loops to get more insights. As listed in Table 1, the resonant frequency of the S_{21} curve (i.e., f_r) varies as the edge-to-edge

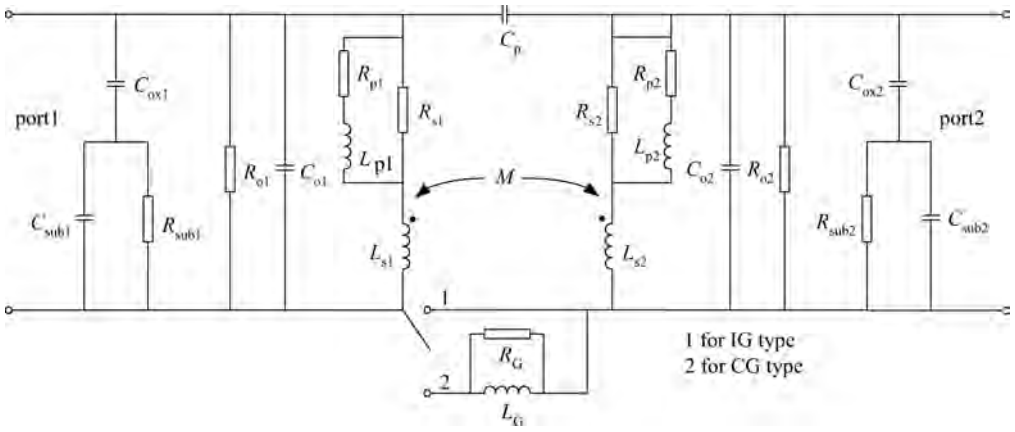

Fig. 5. Compact equivalent circuit model for transformers.

Table 1. Resonant frequencies of S_{21} curves.

f_r (GHz) S_1 (μm) / S_2 (μm)	10	30	50	70	90
10	9.3	9.2	9.1	9.0	8.9
30	9.2	9.1	9.0	8.9	8.8
50	9.1	9.0	8.9	8.8	8.7
70	9.0	8.9	8.8	8.7	8.6
90	8.9	8.8	8.7	8.6	8.5

separation (i.e., S_1 or S_2) changes. It can be concluded that the larger value of S_1+S_2 leads to the lower f_r, and the same value of $S_1 + S_2$ leads to almost the same f_r. From these concluded rules, two points can be inferred as follows.

(1) The grounding strips can induce current loops. The larger the value of $S_1 + S_2$, the larger the loop area becomes. To a certain extent, a larger loop area means larger inductance, and then leads to a lower resonant frequency.

(2) The loop inductors (L_{G1} and L_{G2}) affect the performance of the transformer in the series form rather than the parallel kind. If they are in parallel, the value of $(S_1\times S_2)/(S_1+S_2)$ rather than $S_1 + S_2$ will take effect, then the second rule will not be obeyed.

4. Compact equivalent circuit model

4.1. Model presentation

As shown in Fig. 5, a physics-based equivalent circuit model is proposed to model on-chip spiral transformers. In this model, the sub-network consisting of R_{si}, L_{si}, R_{pi} and L_{pi} (i = 1, 2) is used to account for the skin effect of each coil. C_{subi} and R_{subi} represent the characteristics of the conductive silicon substrate. C_{oxi} models the oxide-layer capacitance between the metal and the substrate. R_{oi} is introduced to account for the spiral coil's conductor loss originated from the lossy substrate return path[10]. C_{oi} denotes the underpass capacitance. The magnetic and electric couplings between two coils are represented by M and C_p, respectively. L_G and R_G account for the additional magnetic coupling and conductor loss introduced by the grounding strips in the CG type, respectively.

4.2. Model parameter extraction

Based on our previous work[11], the parameters of the IG type model can be extracted directly. The direct extraction procedure proposed in Ref. [11] is simply described as follows.

(1) Convert the measured S-parameters to corresponding $ABCD$-parameters. According to the conversion rules between 2-port network parameters, we can get

$$A = \frac{(1+S_{11})(1-S_{22})+S_{12}S_{21}}{2S_{21}}, \tag{1}$$

$$B = Z_0\frac{(1+S_{11})(1+S_{22})-S_{12}S_{21}}{2S_{21}}, \tag{2}$$

$$C = \frac{(1-S_{11})(1-S_{22})-S_{12}S_{21}}{2Z_0S_{21}}, \tag{3}$$

$$D = \frac{(1-S_{11})(1+S_{22})+S_{12}S_{21}}{2S_{21}}, \tag{4}$$

where Z_0 denotes the characteristic impedance of the testing ports.

(2) Determine the value of the element M as

$$M = \left.\frac{\mathrm{Im}[(Z_{12}+Z_{21})/2]}{\omega}\right|_{\omega\to 0}, \tag{5}$$

where Z_{12} and Z_{21} are Z-parameters converted from the measured S-parameters.

(3) Define three admittances: Y_2 (tool admittance), Y_1 (shunt branch admittance) and Y_3 (series branch admittance)

$$Y_2 = 0.5/\mathrm{j}\omega M, \tag{6}$$

$$Y_1 = \frac{A-\sqrt{1+2BY_2}}{B}, \tag{7}$$

$$Y_3 = \frac{1+\sqrt{1+2BY_2}}{B}. \tag{8}$$

(4) Extraction for the shunt branch. The shunt branch is composed of three elements, i.e., C_{oxi}, C_{subi} and R_{subi} (i = 1, 2). Using the real part and imaginary part of the admittance (i.e., Y_1), Reference [12] introduced two useful characteristic functions as

$$f_1(\omega) = \frac{\omega^2}{\mathrm{Re}(Y_1)}, \tag{9}$$

$$f_2(\omega) = \frac{\mathrm{Im}(Y_1)}{\mathrm{Re}(Y_1)}\omega. \tag{10}$$

We directly use the method developed in Ref. [12] to extract the values of C_{oxi}, C_{subi} and R_{subi}, and the detailed process is omitted.

(5) Extraction for the series branch. The series branch consisting of R_{si}, (L_{si}–M), R_{pi} and L_{pi} (i = 1, 2) forms a ladder circuit. The real part and imaginary part of the ladder's impedance (i.e., $Z_s = 1/Y_3$) can be written as

$$\mathrm{rz} = \mathrm{Re}(1/Y_3), \tag{11}$$

$$\mathrm{lz} = \frac{\mathrm{Im}(1/Y_3)}{\omega}. \tag{12}$$

To extract their parameters, we developed two characteristic functions as

$$f_3 = \frac{\omega^2 - \omega_0^2}{(\mathrm{lz}/\mathrm{rz}) - (\mathrm{lz}/\mathrm{rz})_{\omega\to\omega_0}}$$

$$= -\frac{(R_s R_p + R_p^2 + L_p^2\omega^2)(R_s R_p + R_p^2 + L_p^2\omega_0^2)}{L_p^2[L_p R_s + (L_s - M)(R_s + R_p)]}, \tag{13}$$

$$f_4 = \frac{(\omega^2 - \omega_0^2)(\mathrm{lz} - \mathrm{lz}_{\omega\to\omega_0})}{\mathrm{rz} - \mathrm{rz}_{\omega\to\omega_0}}$$

$$= -\frac{L_p(\omega^2 - \omega_0^2)}{R_s + R_p} = q_1 + q_2\omega^2, \tag{14}$$

where ω_0 is the reference frequency and it should be set as the minimum frequency of the measurement in our extraction process.

Using the linear regression technology, the coefficients p_1, p_2, q_1 and q_2 can be extracted with ease. Then, we can obtain the values of R_{si}, L_{si}, R_{pi} and L_{pi} (i = 1, 2) as follows:

$$k = p_2/(p_1 q_2^2) - 1, \tag{15}$$

$$R_{pi} = \mathrm{rz}_{\omega\to 0}(1 + 1/k), \tag{16}$$

$$R_{si} = R_{pi}k, \tag{17}$$

$$L_{pi} = (R_{si} + R_{pi})(-q_2), \tag{18}$$

$$L_{si} = \mathrm{lz}_{\omega\to\omega_0} - L_{pi}R_{si}^2/[(R_{si} + R_{pi})^2 + L_{pi}^2\omega_0^2] + M. \tag{19}$$

(6) Determine the values of remaining elements. We can get the 2-port Y-parameters $[Y^S]$ by simulation with C_p, R_{oi} and C_{oi} (i = 1, 2) neglected and other elements set with values extracted from above steps. $[Y^M]$ denotes the 2-port Y-parameters converted from the measured S-parameters. Then, C_p, R_{oi} and C_{oi} (i = 1, 2) can be extracted at the resonant frequency as

$$C_o = \frac{\mathrm{Im}(Y_{11}^M + Y_{12}^M - Y_{11}^S - Y_{12}^S)}{\omega}, \tag{20}$$

$$R_{oi} = \frac{1}{\mathrm{Re}(Y_{11}^M + Y_{12}^M - Y_{11}^S - Y_{12}^S)}, \tag{21}$$

$$C_{pi} = \frac{\mathrm{Im}(Y_{12}^S - Y_{12}^M)}{\omega}. \tag{22}$$

By following steps (1)–(6), all the parameters of the IG type model have been extracted. To extract the parameters of the CG type model, we directly adopt all the IG type parameters (except C_p). This is due to the fact that the main differences between two types focus on the model elements (C_p, L_G and R_G), which has been discussed in Section 3. To get the value of L_G, the accurate expression proposed by Greenhouse[13] is used to calculate the values of L_{G1} and L_{G2}. Thus, L_G can be set as the sum of L_{G1} and L_{G2}. Then, the value of C_p can be tuned to the state when the CG model's S_{21} curve shares the same resonant frequency with measurements. Finally, we tune the value of R_G so as to make the model's responses approach those from measurements.

Table 2. Extracted model parameters for transformers in different types.

R_{si}	L_{si}	R_{subi}	C_{oi}	C_{oxi}	C_p(IG)	M	R_G
R_{pi} (Ω)	L_{pi} (nH)	R_{oi} (Ω)	(fF)	C_{subi} (fF)	C_p(CG) (fF)	L_G (nH)	(Ω)
82.97	2.93	525.14	9.77	51.59	5.41	2.78	630.19
5.13	0.66	6000		21.06	112.20	1.34	

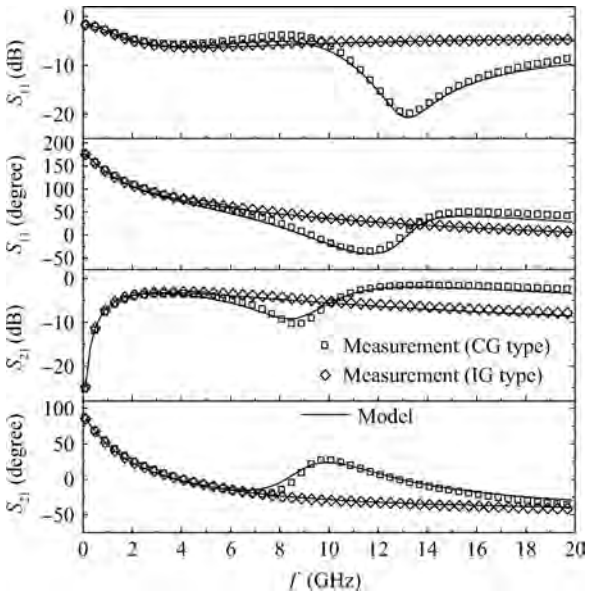

Fig. 6. Model verification.

5. Model verification

After the parameter extraction process, all the model parameters are listed in Table 2. In this table, the CG type model

differs from the IG type: the former has a larger C_p value (about 21 times of the latter) and an additional branch consisting of L_G and R_G. These differences agree well with the analysis in Section 3. In order to verify the model's validity and accuracy, we have compared the modeled and measured S-parameters. As demonstrated in Fig. 6, an excellent agreement has been found over a broad frequency range.

6. Conclusion

Different characteristics have been found when measuring two fabricated on-chip transformers under different ground conditions. Then, the differences are analyzed by EM simulations from the electric and magnetic aspects. A physics-based equivalent circuit model is proposed to model transformers under different ground conditions. The model parameters are extracted and agree with the analysis. To verify the model's accuracy, we have compared the modeled and measured S-parameters, and an excellent agreement has been found.

References

[1] Wang C, Liao H L, Xiong Y Z, et al. A physics-based equivalent-circuit model for on-chip symmetric transformers with accurate substrate modeling. IEEE Trans Microw Theory Tech, 2009, 57(4): 980

[2] Lin Y S, Chen C Z, Liang H B, et al. High-performance on-chip transformers with partial polysilicon patterned ground shields (PGS). IEEE Trans Electron Devices, 2007, 54(1): 157

[3] Howard G E, Dai J, Chow Y L, et al. The power transfer mechanism of MMIC spiral transformers and adjacent spiral inductors. IEEE MTT-S International Microwave Symposium Digest, 1989: 1251

[4] Wei G, Chao J, Tao L, et al. Scalable compact circuit model for differential spiral transformers in CMOS RFICs. IEEE Trans Electron Devices, 2006, 53(9): 2187

[5] El-Gharniti O, Kerherve E, Begueret J B. Modeling and characterization of on-chip transformers for silicon RFIC. IEEE Trans Microw Theory Tech, 2007, 55(4): 607

[6] Lin L, Yin W Y, Mao J F, et al. Performance characterization of circular silicon transformers. IEEE Trans Magnetics, 2008, 44(12): 4684

[7] Lin Y S, Chen C C, Liang H B, et al. A high-performance micromachined RF monolithic transformer with optimized pattern ground shields (OPGS) for UWB RFIC applications. IEEE Trans Electron Devices, 2007, 54(3): 609

[8] Chong K, Xie Y H. High-performance on-chip transformers. IEEE Electron Device Lett, 2005, 26(8): 557

[9] El-Gharniti Q, Kerherve E, Begueret J B. Design and modeling of on-chip monolithic transformers with patterned ground shield. Proceedings IEEE International Symposium on Circuits and Systems, 2006

[10] Guo J C, Tan T Y. A broadband and scalable model for on-chip inductors incorporating substrate and conductor loss effects. IEEE Trans Electron Devices, 2006, 53(3): 413

[11] Wei Jiaju, Wang Zhigong, Li Zhiqun. Direct extraction of equivalent circuit parameters for on-chip spiral transformers. Journal of Semiconductors, 2012, 33(1): 015012

[12] Huang F, Lu J, Jiang N, et al. Frequency-independent asymmetric double-π equivalent circuit for on-chip spiral inductors: physics-based modeling and parameter extraction. IEEE J Solid-State Circuits, 2006, 41(10): 2272

[13] Greenhouse H. Design of planar rectangular microelectronic inductors. IEEE Trans Parts, Hybrids, and Packaging, 1974, 10(2): 101